Journal of Catalysis 258 (2008) 296–305

Contents lists available at ScienceDirect

Journal of Catalysis

www.elsevier.com/locate/jcat

Kinetics of the NO/H_2 reaction on $Pt/LaCoO_3$: A combined theoretical and experimental study

F. Dhainaut [a,c], S. Pietrzyk [a,b,c], P. Granger [c,*]

[a] Ecole Nationale Supérieure de Chimie de Lille, 59655-Villeneuve d'Ascq, France
[b] Ecole Centrale de Lille, 59655-Villeneuve d'Ascq, France
[c] Unité de Catalyse et de Chimie du Solide, UMR CNRS N° 8181, Bâtiment C3, Université des Sciences et Technologies de Lille, 59655-Villeneuve d'Ascq, France

ARTICLE INFO

Article history:
Received 26 March 2008
Revised 14 June 2008
Accepted 4 July 2008
Available online 30 July 2008

Keywords:
Platinum
Low-temperature NO_x reduction process
Hydrogen
N_2O selectivity
Kinetics
Reaction mechanism

ABSTRACT

This paper reports an extensive kinetic investigation of the overall reduction of NO by H_2 over platinum supported on $LaCoO_3$. Particular attention has been given to the influence of reductive pretreatment under pure H_2 at 250 or 450 °C. According to temperature conditions, a partial or extensive reduction of the support occurs that drastically changes the kinetic behaviour. Prereduction at 250 °C leads to metallic platinum particles in weak interaction with $LaCoO_3$. In that case, only Pt catalyses the NO/H_2 reaction, which obeys a conventional Langmuir–Hinshelwood mechanism. On the other hand, extensive reduction of $LaCoO_3$ into La_2O_3 and CoO_x ($x < 1$) at 450 °C leads to peculiar interactions between metallic Pt particles and CoO_x, correlated with different kinetics features. A bifunctional mechanism involving anionic vacancies at the vicinity of platinum particles likely occurs. Subsequent comparisons of adjusted kinetic and thermodynamic constants on supported Pt and Pd explain the changes in their intrinsic catalytic performance.

1. Introduction

Today, research efforts are essentially focused on the development of low atmospheric pollutant emission systems, integrating low energy consumption to minimise CO_2 emissions and other gases that exhibit greenhouse gas behaviour. Such a viewpoint must be taken into account for future implementation of efficient catalytic end-of-pipe technologies devoted to nitric oxide (NO_x) abatement.

Previous investigations underlined the potential interest of hydrogen as reducing agent for the catalytic reduction of NO_x in three-way conditions and in O_2 excess [1–10]. Findings from those investigations showed that NO can be efficiently reduced to N_2 at moderate temperature ($T > 100$ °C), particularly on noble metals supported on reducible materials, such as perovskites [1,3–7,9]. Such efficiency is related to the specific interactions between noble metals and perovskites according to reactive conditions. Reversible structural changes have been reported after exposure to reductive or oxidative atmosphere, which may generate synergistic effects on the selective conversion of NO_x to nitrogen on Pt and Pd [1,7,10,11], particularly on $LaCoO_3$ [6,7,11–13]. Previous investigations dealt with the kinetics of the NO/H_2 reaction in the absence of oxygen on supported Rh-, Pt-, and Pd-based catalysts [14–18]. In fact, various reactions may occur over noble metals with the simultaneous formation of N_2, N_2O, and NH_3 according to the following set of reactions:

$$2NO + 2H_2 = N_2 + 2H_2O, \quad (1)$$

$$2NO + H_2 = N_2O + H_2O, \quad (2)$$

$$2NO + 5H_2 = 2NH_3 + 2H_2O. \quad (3)$$

Among the different mechanism proposals, there are controversial aspects concerning the nature of elementary steps related to the formation of nitrogen, as well as the nature of intermediates, because nitrosyl, dinitrosyl, nitrites, and nitrates can be involved [12–14,16–18]. By way of illustration, Burch et al. [18] suggested the involvement of the gas-phase or very weakly adsorbed NO species for the formation of N_2O on Pt, whereas chemisorbed N atoms and NO molecules recombine for the formation of N_2 [16]. Alternative explanations were recently proposed for the reduction of NO by H_2 on Pd/Al_2O_3 [12,13]. A bimolecular reaction between two adjacent adsorbed NO molecules for the production of N_2O was proposed according to the following step:

$$NO_{ads} + NO_{ads} \rightarrow N_2O + O_{ads}. \quad (4)$$

Previous steady-state rate measurements performed in our laboratory on Pd/Al_2O_3 agree with mechanism 1 described in Fig. 1 [12,13]. Two important mechanistic information arise in this sequence, associated with NO dissociation assisted by hydrogen, as suggested

* Corresponding author. Fax: +33 3 20 43 65 61.
E-mail address: pascal.granger@univ-lille1.fr (P. Granger).

0021-9517/$ – see front matter
doi:10.1016/j.jcat.2008.07.003

Mechanism 1		Mechanism 2	
$NO + * \leftrightarrows NO_{ads}$	(5)	$NO + * \leftrightarrows NO_{ads}$	(5)
$H_2 + 2* \leftrightarrows 2H_{ads}$	(6)	$H_2 + 2* \leftrightarrows 2H_{ads}$	(6)
$NO_{ads} + H_{ads} \rightarrow N_{ads} + OH_{ads}$	(7)	$O + H_{ads} \rightarrow OH + *$	(16)
$N_{ads} + N_{ads} \rightarrow N_2 + 2*$	(8)	$OH + H_{ads} \rightarrow H_2O + V + *$	(17)
$NO_{ads} + N_{ads} \rightarrow N_2 + O_{ads} + *$	(9)	$V + NO_{ads} \rightarrow O + N_{ads}$	(18)
$NO_{ads} + N_{ads} \rightarrow N_2O + 2*$	(10)	$N_{ads} + N_{ads} \rightarrow N_2 + 2*$	(8)
$N_{ads} + H_{ads} \rightarrow NH_{ads} + *$	(11)	$NO_{ads} + N_{ads} \rightarrow N_2 + O_{ads} + *$	(9)
$NH_{ads} + H_{ads} \rightarrow NH_{2,ads} + *$	(12)	$NO_{ads} + N_{ads} \rightarrow N_2O + 2*$	(10)
$NH_{2,ads} + H_{ads} \rightarrow NH_3 + 2*$	(13)	$N_{ads} + H_{ads} \rightarrow NH_{ads} + *$	(11)
$O_{ads} + H_{ads} \rightarrow OH_{ads} + *$	(14)	$NH_{ads} + H_{ads} \rightarrow NH_{2,ads} + *$	(12)
$OH_{ads} + H_{ads} \rightarrow H_2O + 2*$	(15)	$NH_{2,ads} + H_{ads} \rightarrow NH_3 + 2*$	(13)
		$O_{ads} + H_{ads} \rightarrow OH_{ads} + *$	(14)
		$OH_{ads} + H_{ads} \rightarrow H_2O + 2*$	(15)

Fig. 1. Mechanism schemes for the NO/H_2 reaction on Pd/Al_2O_3 (mechanism 1) and on $Pd/LaCoO_3$ [12,13].

earlier by Hecker and Bell [see step (7)] [14], whereas previous investigations privileged a nearest-neighbour vacant site for NO_{ads} dissociation according to step (19):

$$NO_{ads} + * \rightarrow N_{ads} + O_{ads}. \quad (19)$$

Different kinetic features were reported on $Pd/LaCoO_3$ with alternative mechanistic proposals involving the redox properties of the support according to mechanism 2 (see Fig. 1). As indicated, oxygen species (O) from the support may react with hydrogen, and then NO would dissociate on anionic vacancies (V) subsequently formed according to steps (16)–(18).

This study deals with a combined theoretical and experimental kinetic study of the NO/H_2 reaction on $Pt/LaCoO_3$. Subsequent comparisons with Pd-based catalysts will show different selectivity behaviours toward the transformation of NO into nitrogen, which have been explained by the involvement of different elementary steps.

2. Experimental

2.1. Catalyst preparation and characterisation

$LaCoO_3$ (20 $m^2\,g^{-1}$) was prepared according to a so-called "sol–gel" method involving a citrate route [4,19]. Optimal textural and structural properties were obtained after exposure to air at 600 °C. Platinum deposition on $LaCoO_3$ was achieved according to a classical wet impregnation route using hexachloroplatinic acid solutions with adjusted concentrations to obtain 1 wt% Pt. The impregnated samples were calcined in air at 400 °C and then reduced overnight at 250 or 450 °C in pure H_2. The respective catalysts were designated $Pt/LaCoO_3(250)$ and $Pt/LaCoO_3(450)$. Pt dispersion was obtained from H_2 titration performed at room temperature. The hydrogen uptake calculated from H_2 chemisorption measurements on $Pt/LaCoO_3(450)$ was 2.5 µmol per gram of catalyst corresponding to a metallic Pt dispersion of 0.06. Previous investigations [5,20] found the occurrence of hydrogen spillover effects during H_2 chemisorption measurements, particularly when noble metals were dispersed on reducible materials. The corresponding value on $Pt/LaCoO_3(250)$ was not reported due to significant overestimation. In fact, H_2 spillover strongly depended on the reductive pretreatment in H_2. It was found that the intensity of these hydrogen transfer phenomena was decreased with increasing reduction temperature of Pd supported on ceria–zirconia mixed oxides [20]. Such a process could not be strictly ruled out after extensive reduction at 450 °C. Additional experiments on reduced $LaCoO_3$ support did not show a significant hydrogen uptake (<0.1 µmol per gram of catalyst).

H_2 temperature-programmed reduction (TPR) experiments were carried out on a Micromeritics Autochem II 2920 instrument under a flow of 5 vol% H_2 diluted in Ar. In situ X-ray diffraction (XRD) patterns were recorded on a Bruker D8 diffractometer using Cu$K\alpha$ ($\lambda = 0.154$ nm) radiation. The sample was reduced in situ under a flow of 3 vol% H_2 diluted in He. The temperature gradually increased to the desired temperature at a heating rate $dT/dt = 3\,°C\,min^{-1}$. Data acquisition was performed under isothermal conditions. X-ray photoelectron spectroscopy (XPS) experiments were performed using a Vacuum Generators Escalab 220XL spectrometer with a monochromatized aluminium source (1486.6 eV). All binding energies (BEs) were referenced to the BE of C 1s core level (285.1 eV).

2.2. Kinetic measurements

Catalytic measurements were performed in a recycling fixed-bed flow reactor running at atmospheric pressure with a recycling ratio of 180, which created a CSTR performance. The catalytic setup has been described elsewhere [21]. Previous steady-state experiments did not demonstrate any changes in rate measurements from modifying the catalyst loading, suggesting that external diffusion phenomena were minimised. The absence of significant internal diffusion also was checked according to the estimate of the effectiveness factor in our experimental conditions. A value close to 1 was calculated assuming a Knudsen regime with an effective diffusion coefficient $D_{eff} \cong 10^{-6}\ m^2\,s^{-1}$ [22]. Consequently, our steady-state rate measurements were performed under a chemical regime. The catalyst was in powder form, with an average grain size of 80 µm. The gaseous mixture was analysed using a *Balzers* quadrupole mass spectrometer and a *Hewlett Packard 5890 series II* chromatograph fitted with a thermal conductivity detector. Reactants and products were separated on a *CTR1* column supplied by *Alltech*. Typically, catalytic measurements were performed with 0.1 g of catalyst, diluted with 0.2 g of α-Al_2O_3, at a global flow rate of 10 $L\,h^{-1}$. Before reaction, the catalyst samples were reduced in situ in hydrogen at 250 or 450 °C.

The overall conversion of NO (X_{NO}) was calculated according to Eq. (20),

$$X_{NO} = \frac{2(F_{N_2} + F_{N_2O}) + F_{NH_3}}{F^0_{NO}} = X_{N_2} + X_{N_2O} + X_{NH_3}, \quad (20)$$

where X_{NH_3}, X_{N_2}, and X_{N_2O} represent the conversion of NO into ammonia, nitrogen, and nitrous oxide, respectively; F^0_{NO} is the inlet molar flow rate of NO; and F_{NH_3}, F_{N_2} and F_{N_2O} are the molar flow rates of NH_3, N_2, and N_2O, respectively:

The specific rate was calculated according to Eq. (21):

$$r = \frac{F^0_{NO} X_{NO}}{m}\ (mol\,h^{-1}\,g^{-1}), \quad (21)$$

where m is the mass of catalyst. The N_2O-selectivity corresponding to the transformation of NO into N_2O (S_{N_2O}), given by Eq. (22), was easily related to the relative rates r_{N_2}/r_{N_2O} and r_{NH_3}/r_{N_2O}:

$$S_{N_2O} = \frac{2r_{N_2O}}{2r_{N_2O} + 2r_{N_2} + r_{NH_3}} = \frac{1}{1 + \frac{r_{N_2}}{r_{N_2O}} + \frac{r_{NH_3}}{2r_{N_2O}}}, \quad (22)$$

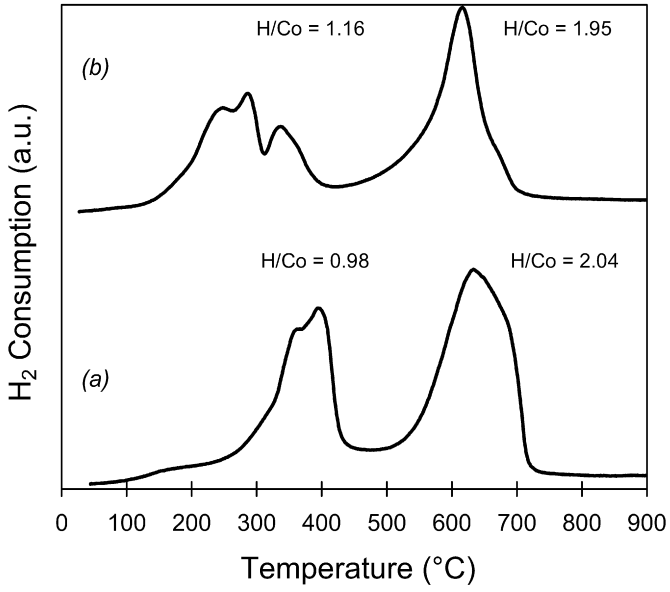

Fig. 2. Temperature-programmed reduction on calcined $LaCoO_3$ (a) and $Pt/LaCoO_3$ (b) under 5 vol% H_2 diluted in Ar.

where r_{N_2}, r_{NH_3} and r_{N_2} are the rates of conversion of NO to N_2O, NH_3, and N_2 respectively.

3. Results

3.1. Effect of reductive preactivation thermal treatment on the bulk and surface physicochemical properties of $Pt/LaCoO_3$

3.1.1. Bulk properties

The reducibility of $LaCoO_3$ was investigated using H_2 TPR experiments. H_2 consumption profiles are reported in Fig. 2. As observed, a two-step reduction process [23] occurred on $LaCoO_3$ with two H_2 consumptions in the temperature ranges 250–450 and 500–730 °C, corresponding to bulk atomic H/Co ratios of 0.98 and 2.04. The global ratio indicates a complete reduction of Co^{3+} species into metallic Co particles involving a two-step process with the intermediate formation of Co^{2+}. Similar tendencies were observed after incorporation of Pt, with a significant shift of the low H_2-temperature consumption range to lower temperatures. The overestimation of the atomic H/Co ratio of >1 is connected to additional reduction of PtO_2 into Pt^0. In situ XRD measurements were performed under reductive conditions in the presence of 3 vol% H_2 diluted in He between room temperature and 800 °C. XRD patterns recorded on the calcined $PtO_2/LaCoO_3$ indicate that a two-step reduction process occurred. As illustrated in Fig. 3, the most intense characteristic X-ray line of the rhombohedral structure of $LaCoO_3$, at $2\theta = 32.9$, shifted progressively toward lower values up to 500 °C due to partial reduction of Co(III) located in B sites of the perovskite structure. Subsequent temperature increases above 500 °C led to the disappearance of X-ray lines characteristic of $LaCoO_3$. Correlatively, additional contributions developed at $2\theta = 26.2°, 29.2°, 29.9°, 46.2°, 52.3°$, and 55°, assigned to the hexagonal structure of La_2O_3. Interestingly, no related bulk cobalt structure was detected, suggesting a high degree of dispersion of reduced cobalt species. Ex situ XRD measurements on $Pt/LaCoO_3(450)$ indicated an extensive bulk reduction during reductive thermal treatment overnight at 450 °C, leading to the disappearance of $LaCoO_3$. In contrast, the structural properties of $LaCoO_3$ were preserved at 250 °C.

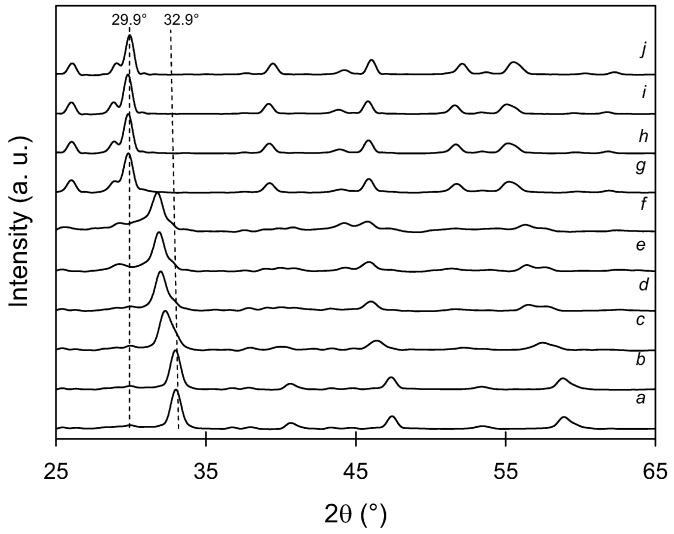

Fig. 3. In situ XRD analysis of calcined $Pt/LaCoO_3$ during reductive thermal treatment in 3 vol% H_2 diluted in He: 25 (a), 100 (b), 200 (c), 300 (d), 400 (e), 500 (f), 600 (g), 700 (h), 800 °C (i), after cooling down at room temperature (j).

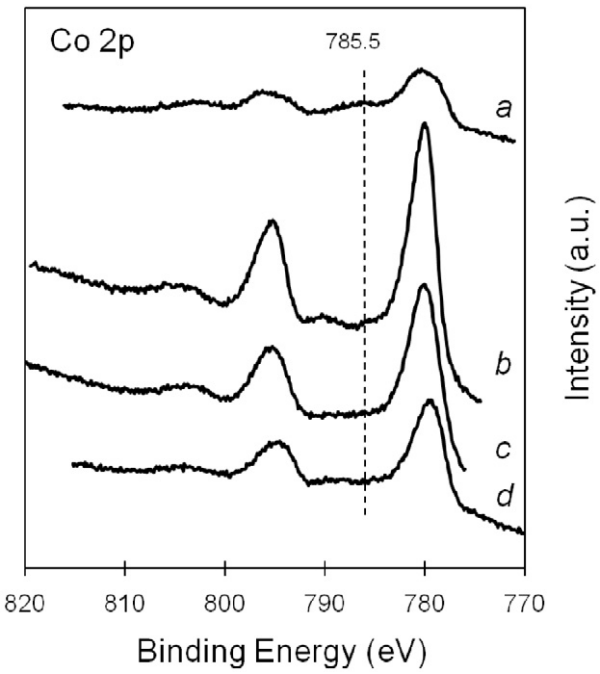

Fig. 4. Co 2p spectra from ex situ XPS analysis on $Pt/LaCoO_3(250)$ (a), $Pt/LaCoO_3$-(250) after steady-state measurements (b), $Pt/LaCoO_3(450)$ (c), $Pt/LaCoO_3(450)$ after steady-state measurements (d).

3.1.2. Surface properties

Ex situ XPS measurements were performed on both freshly prepared and used $Pt/LaCoO_3(250)$ and $Pt/LaCoO_3(450)$ after kinetic measurements. Co 2p spectra are shown in Fig. 4, and spectroscopic features are summarised in Table 1. In all cases, partial surface oxidation due to storage at room temperature must be accounted for, because no subsequent in situ thermal treatment was performed before XPS analysis. Changes in spectral features after reaction were observed predominately on $Pt/LaCoO_3(250)$, with a narrower Co 2p photo peak exhibiting a half-peak width of 3.4, versus 5.2 before reaction. Parallel to those observations, a strong attenuation of the characteristic shakeup structure at 785.5 usually assigned to Co^{2+} was seen, along with a weak and broad signal at 789.7 eV corresponding to the usual shakeup structure of Co^{3+}. Re-

Table 1
Ex situ XPS analysis of Pt supported on $LaCoO_3$ submitted to different thermal treatment

Catalyst		B.E. (eV)[a] Co $2p_{3/2}$	Half-peak width (eV)	Surf. Co composition[b] Co/La
$Pt/LaCoO_3(250)$	Initial	780.3	5.2	0.59
	After reaction[c]	780.1	3.4	0.67
$Pt/LaCoO_3(450)$	Initial	779.7	3.8	0.59
	After reaction[c]	780.1	4.0	0.57

[a] Binding energy (accuracy ± 0.2 eV).
[b] Relative accuracy equal to ±20% on the atomic Co/La ratio.
[c] Reaction conditions: T (reaction) = 145 °C, inlet partial pressures of H_2 and NO in the range $(4.3–11.7) \times 10^{-3}$ and $(2.8–12.6) \times 10^{-3}$ atm respectively.

Table 2
Calculated enthalpies (ΔH) and activation barriers (ΔE) in kJ mol^{-1} for various elementary steps suggested in the NO + H_2 reaction on Pt(111) and Pd(111)

Reaction	Pt(111)		Pd(111)	
	ΔH	ΔE	ΔH	ΔE
$NO_g + * \rightarrow NO_{ads}$	−109	0	−134	0
$H_{2g} + * \rightarrow H_{2ads}$	−27	0	−28	0
$H_{2g} + 2* \rightarrow 2H_{ads}$	−75	13	−84	9
$O_{2g} + 2* \rightarrow 2O_{ads}$	−213	0	−232	0
$NO_{ads} + * \rightarrow N_{ads} + O_{ads}$	−100	53	−143	38
$NO_{ads} + H_{ads} \rightarrow N_{ads} + OH_{ads}$	−78	22	−114	7
$NO_{ads} + H_{ads} \rightarrow NH_{ads} + O_{ads}$	32	96	1	89
$NO_{ads} + H_{2ads} \rightarrow NH_{ads} + OH_{ads}$	5	55	−25	44
$2N_{ads} \rightarrow N_{2g} + 2*$	25	111	142	179
$NO_{ads} + N_{ads} \rightarrow N_{2g} + O_{ads} + *$	−75	7	−1	53
$NO_{ads} + N_{ads} \rightarrow N_2O_g + 2*$	113	113	197	197
$NO_{ads} + N_{ads} \rightarrow N_2O_{ads} + *$	72	81	142	142
$N_2O_{ads} \rightarrow N_2O_g + *$	41	41	55	55
$N_2O_{ads} \rightarrow N_{2ads} + O_{ads}$	−132.3	0	−287.4	0
$N_{2ads} \rightarrow N_{2ads} + *$	45.2	45.2	56	56
$NO_{ads} + NH_{ads} \rightarrow N_{2g} + OH_{ads}$	−185	0	−116	0
$NO_{ads} + NH_{ads} \rightarrow N_2O_g + H_{ads}$	−19	30	52	74
$2NO_{ads} \rightarrow N_2O_g + O_{ads} + *$	13	34	54	60
$N_{ads} + H_{ads} \rightarrow NH_{ads} + *$	132	150	143	159
$N_{ads} + H_{2ads} \rightarrow NH_{ads} + H_{ads}$	83	110	88	118
$NH_{ads} + H_{ads} \rightarrow NH_{2ads} + *$	−41	48	−25	61
$NH_{2ads} + H_{ads} \rightarrow NH_3 + 2*$	−7	23	36	44
$O_{ads} + H_{ads} \rightarrow OH_{ads} + *$	22	85	29	91
$OH_{ads} + H_{ads} \rightarrow H_2O_g + 2*$	−77	0	−66	0
$O_{ads} + H_{2ads} \rightarrow OH_{ads} + H_{ads}$	−26	139	−27	137

garding $Pt/LaCoO_3(450)$, no significant change in spectral features was seen on the used catalyst, which may be related to subsequent modifications under reactive conditions. Also, no significant signal was detected on the N 1s photo peak, which may be related to significant accumulation of nitrites/nitrates in the course of the reaction.

3.2. Kinetics of the NO/H_2 reactions

3.2.1. Theoretical approach

Theoretical and practical approaches were compared to evaluate the validity of key elementary steps related to the transformation of NO in mechanism 1, as proposed previously on Pd/Al_2O_3. The bond order conservation Morse potential and its generalisation as the unity bond index–quadratic exponential potential (UBI-QEP), developed by Shustorovich et al. [24–26], can be used for this purpose. This mathematical model straightforwardly provides the heat of adsorption for molecular and radical species and the activation barrier for elementary reactions. Estimated data for elementary $DeNO_x$ reactions, such as decomposition and/or reduction to N_2, N_2O, and NH_3, were previously reported on closely packed surface Pt(111) [25]. In the present work, those calculations were completed on Pd(111), taking into account various proposals in the literature, including a bimolecular reaction between two chemisorbed NO molecules and between adsorbed NO and NH_x species according to previous suggestions [17,18], and were repeated on Pt(111) (see Table 2). The model input parameters, dissociation energies, and atomic heats of adsorption were obtained from previous work [24]. N_2O was treated according to Zeigarnik's approach [28]. This approach integrates the heat of adsorption in the zero coverage limit case, which does not reflect our typical reactive conditions. Similar calculations also account for NO bonded via the N atom at a two-fold bridge site. As observed, the deviation between the enthalpies of NO and H_2 on Pd(111), −134 and −28 kJ mol^{-1}, respectively, at $\theta = 0$, leads to the conclusion that the competition for adsorption on Pd(111) was largely in favour of NO. Such a tendency was observed on Pt(111), but to a lesser degree. Consider that under realistic conditions, at high coverage, a weakening of the metal–adsorbate bond would be expected due to lateral repulsive interactions and changes in the coordination mode of adsorbates [24]. By way of illustration, on-top coordination may be more representative at high coverage for NO adsorption on Pt(111) [27]. Consequently, experimental values derived from kinetic experiments should be lower than theoretical ones. Such a tendency was previously reported for the NO/H_2 reaction on Pd [13]. Considering the particular case of H_2 adsorption on NO saturated surfaces, in agreement with the calculated adsorption enthalpies, the probability for finding two adjacent sites for the dissociative adsorption would be very low, particularly on Pd(111). Consequently, weakly bonded chemisorbed H atoms and H_2 molecules were envisaged as intermediates. As indicated in Table 2, different cases were examined for the dissociation of chemisorbed NO molecules involving nearest-neighbour vacant sites (step (19)) and assisted by dissociated or molecular

chemisorbed hydrogen species. In this latter case, the occurrence of different routes can be considered according to steps (23)–(25). As shown, the activation barrier for step (24) on Pt(111) was significantly higher than that obtained according to step (23) (96 vs 22 kJ mol^{-1}) and remained higher than that calculated for the dissociation of NO on a nearest-neighbour vacant site (53 kJ mol^{-1}). Similar trends were observed on Pd(111). The involvement of molecular H_2 precursor also was considered; however, calculations led to a slightly higher activation barrier then those obtained when NO_{ads} dissociated on a nearest-neighbour vacant site. Consequently, these findings suggest that dissociated hydrogen species on Pt(111) and Pd(111) surfaces assist in the dissociation of NO on Pt(111) and Pd(111) rather than the molecular precursor:

$$NO_{ads} + H_{ads} \rightarrow N_{ads} + OH_{ads}, \quad (23)$$

$$NO_{ads} + H_{ads} \rightarrow NH_{ads} + O_{ads}, \quad (24)$$

$$NO_{ads} + H_{2,ads} \rightarrow NH_{ads} + OH_{ads}. \quad (25)$$

We next examine the subsequent production of nitrogen from adsorbed N-containing species. Particular attention can be given to the production of nitrogen, the target molecule. Two different reaction pathways involving adsorbed N atoms can be considered related to the usual associative desorption of nitrogen ($N_{ads} + N_{ads} \rightarrow N_2 + 2*$) and the subsequent step (9) ($NO_{ads} + N_{ads} \rightarrow N_2 + O_{ads} + *$) as reported in Fig. 1 and Table 2. A significantly higher activation barrier was obtained for the former step on Pd (179 vs 53 kJ mol^{-1}) and on Pt (111 vs 7 kJ mol^{-1}), suggesting that N_2 would form preferentially via step (9). Previous kinetic measurements on supported polycrystalline Pd corroborate these theoretical calculations [12,13]. It was found that steps (9) and (10) predominated for the formation of N_2 and N_2O, respectively. We evaluated alternative routes that account for the involvement of chemisorbed N_2O molecules as common intermediates for the production of N_2O and N_2 via the desorption or dissociation of adsorbed N_2O molecules, respectively, and reached the same conclusion by comparing the activation barriers associated with steps for the production of N_2O and N_2. In both cases, the preferential formation of nitrogen would be expected. An ultimate attempt takes into account the formation of N_2O via a bimolecular reaction between two adjacent chemisorbed NO molecules. Such a reaction pathway was suggested previously [13,17,18] and should be taken into account in the case of surfaces essentially covered by NO_{ads}. The calculated activation barriers of 60 and 44 kJ mol^{-1} on Pd(111) and Pt(111), respectively, were relatively low, suggesting that this step could compete with step (10) for the production of N_2O. However, such a suggestion disagrees with the relative insensitivity of the N_2O selectivity to reaction conditions and the negative apparent order with respect to the partial pressure of NO reported previously on Pd [12,13].

We next consider the formation of ammonia. The results presented in Table 2 indicate that the hydrogenation of N_{ads} to NH_{ads} was rate-limited, with higher activation energies of 150 and 159 kJ mol^{-1} on Pt(111) and Pd(111), respectively, than those corresponding to the successive hydrogenation steps of NH_{ads} species to NH_3. Additional calculations involving bimolecular reactions between chemisorbed NO and NH_{ads} species were considered for the production of N_2 and N_2O with lower numerical solutions for ΔE than those calculated accounting for N_{ads} as an intermediate. However, it is noteworthy that the activation barrier for N_2 production remained lower than that calculated for N_2O, indicating that N_2 would be formed preferentially at the expense of N_2O via the involvement of NH_{ads} species.

3.2.2. Experimental approach

Preliminary temperature-programmed experiments Earlier investigations of the NO/H_2 reaction [6] showed that $LaCoO_3$ exhibits significant catalytic activity in the conversion of NO above 300 °C. As illustrated in Fig. 5, a subsequent incorporation of platinum drastically increased the activity with conversion starting above 50 °C. In addition, significant changes in the conversion profiles of NO according to the temperature of the reductive pretreatment occurred. As shown in Fig. 5, a maximum NO conversion occurred at 205 °C on Pt/$LaCoO_3$(250). Above that temperature, NO conversion decreased gradually. This finding is related to competitive processes with side reactions involving the catalysts. As shown previously, prereduction at 250 °C did not alter the bulk structural properties of $LaCoO_3$ with the stabilisation of partially reduced Co^{2+} species. Consequently, additional consumption of hydrogen could occur above 205 °C during temperature-programmed experiments, likely due to extra reduction of Co^{2+} species to metallic Co particles at the expense of NO reduction. As shown in Fig. 6, similar bulk processes also occurred on Pd/$LaCoO_3$(250). A different con-

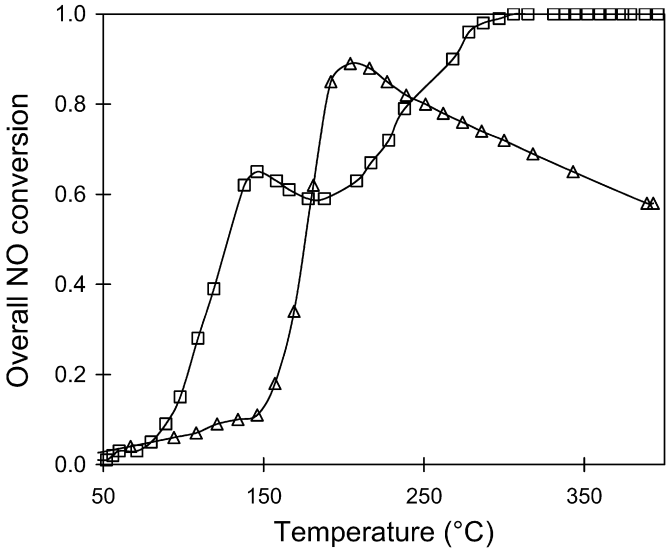

Fig. 5. Temperature-programmed conversion curves of NO by reaction with H_2 on Pt/$LaCoO_3$(250) (□) and Pt/$LaCoO_3$(450) (△) with identical inlet H_2 and NO partial pressures of 1×10^{-2} atm.

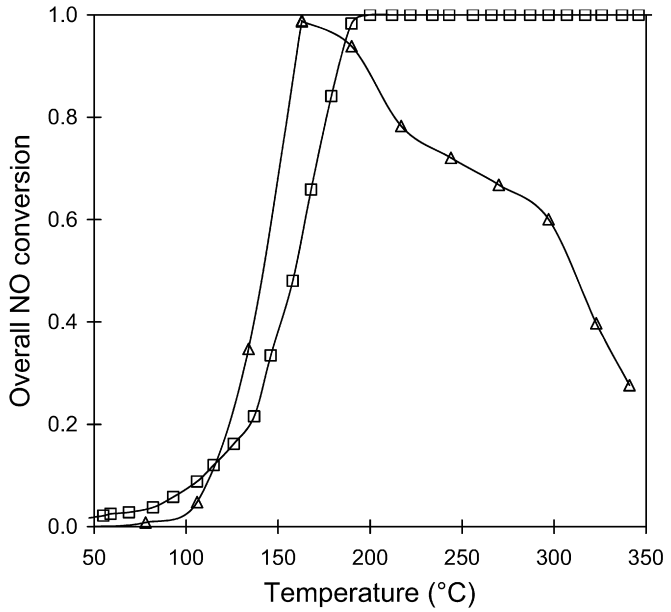

Fig. 6. Temperature-programmed conversion curves of NO by reaction with H_2 on Pd/$LaCoO_3$(250) (□) and Pd/$LaCoO_3$(450) (△) with identical inlet H_2 and NO partial pressures of 1×10^{-2} atm.

Table 3
Partial pressure dependence on the catalytic performances of $Pd/LaCoO_3(250)$ in the $NO + H_2$ reaction $-T$ (reaction) = 145 °C

pNO (10^{-3} atm)	pH_2 (10^{-3} atm)	r (10^{-3} mol h^{-1} g^{-1})	r_{N_2}/r_{N_2O}	r_{NH_3}/r_{N_2O}
7.8	7.9	9.0	0.46	0.24
11.5	7.3	10.3	0.42	0.42
10.6	8.1	9.8	0.41	0.12
2.8	7.0	–	0.80	1.08
4.2	6.6	7.4	0.71	0.95
12.0	6.9	6.1	0.40	0.35
9.1	8.1	9.4	0.43	0.03
4.7	5.7	–	0.57	0.70
8.3	4.8	6.9	0.34	0.45
8.4	4.3	6.5	0.38	0.37
7.6	11.7	10.4	0.41	1.13
8.0	6.5	8.5	0.47	0.57
7.7	9.8	9.6	0.43	0.23
7.5	8.1	8.8	0.48	0.54
7.8	7.8	10.2	0.47	0.24

Table 4
Partial pressure dependence on the catalytic performances of $Pd/LaCoO_3(450)$ in the $NO + H_2$ reaction $-T$ (reaction) = 145 °C

pNO (10^{-3} atm)	pH_2 (10^{-3} atm)	r (10^{-3} mol h^{-1} g^{-1})	r_{N_2}/r_{N_2O}	r_{NH_3}/r_{N_2O}
9.5	9.3	2.2	0.25	0.56
9.7	6.8	1.7	0.23	0.51
9.6	5.5	1.6	0.27	0.52
9.6	8.5	1.7	0.22	0.50
9.4	11.2	2.6	0.22	0.62
9.4	10.3	2.3	0.25	0.64
9.5	9.3	2.3	0.20	0.76
4.4	9.1	2.5	0.53	1.28
13.5	9.3	1.9	0.19	0.73
6.4	9.1	2.6	0.23	0.66
12.6	9.5	1.8	0.24	0.46
5.3	8.9	3.0	0.34	1.10
14.5	9.2	2.1	0.24	0.58
8.6	9.5	2.2	0.25	0.32
11.5	9.4	1.9	0.21	0.52
7.4	9.3	2.5	0.31	0.73
10.5	9.3	2.2	0.24	0.73
9.5	9.3	2.2	0.30	0.98

version profile characterised $Pt/LaCoO_3(450)$. Under those preactivation conditions, complete reduction of the solid was achieved, and no side reaction related to subsequent processes involving the solid would be expected. However, two distinct conversion ranges were seen with an apparent maximum at 140 °C, which can be attributed to the existence of different kinetic regimes. Such activity changes were not accompanied by the production of NO_2. We note that conversion range on $Pt/LaCoO_3(450)$ between 50 and 175 °C was strongly attenuated on $Pt/LaCoO_3(250)$. As shown in Fig. 6, $Pd/LaCoO_3(450)$ behaved differently with the observation of only one conversion range.

Steady-state rate measurements on $Pt/LaCoO_3$ during the NO/H_2 reaction The temperature dependency of the rate of NO conversion was studied in the range 140–160 °C with identical inlet partial pressures of NO and hydrogen of 1.0×10^{-2} atm. The apparent activation energies of 46.0 and 52.8 kJ mol^{-1} on $Pt/LaCoO_3(450)$ and $Pt/LaCoO_3(250)$, respectively, were estimated from the slope of the Arrhenius plots. The influence of NO and H_2 partial pressures was evaluated under isothermal conditions at 145 °C on $Pt/LaCoO_3(250)$ and $Pt/LaCoO_3(450)$ with inlet H_2 and NO partial pressures varying within the ranges $(5.0–15.0) \times 10^{-3}$ and $(2.0–15.0) \times 10^{-3}$ atm, respectively. The experimental rates are reported in Tables 3 and 4. Regarding the N_2O selectivity related to the relative rates r_{N_2}/r_{N_2O} and r_{NH_3}/r_{N_2O}, the formation of N_2O and ammonia was greater on $Pt/LaCoO_3(450)$ than on $Pt/LaCoO_3(250)$. Clearly, the reductive pretreatment at 450 °C had a detrimental effect on the conversion of NO to N_2.

4. Discussion

Activity and selectivity changes in the course of the NO/H_2 reaction on prereduced $Pt/LaCoO_3$ are in qualitative agreement with previous observations from steady-state and transient experiments on Pt/SiO_2 [18]. N_2O formed predominately at low conversion and temperature, whereas N_2 formation was increased above the light-off temperature when the successive reduction of N_2O became significant (results not shown). Ammonia was observed under our operating conditions, with more extensive formation on $Pt/LaCoO_3(450)$ than on $Pt/LaCoO_3(250)$. According to the temperature of the reductive pretreatment in hydrogen at 250 or 450 °C, the preservation of the perovskite structure or its complete reduction with subsequent segregation of La_2O_3 and CoO_x could occur. Consequently, different interactions between metallic Pt particles and the reduced support could explain changes in the kinetic behaviour of both catalysts in terms of activity and selectivity. Such arguments are in line with previous findings on $Pt/CoO_x/SiO_2$ [29] suggesting the involvement of Co species in $DeNO_x$ reactions. However, the relative activity of oxidic cobalt species could be closely related to the oxidation state. As reported previously [30], Co^{3+} was less active than Co^{2+}. Interestingly, $Pt/LaCoO_3(450)$ exhibited two distinct conversion ranges, in contrast to $Pt/LaCoO_3(250)$, with a minimum located at 180 °C (see Fig. 5). This finding may reflect the existence of two different kinetic regimes according to temperature conditions.

Considering the foregoing findings, two main questions arise for modelling our results, concerning the nature of active sites and the nature of elementary steps for the production of N_2O, N_2, and NH_3 on $Pt/LaCoO_3$. Both aspects have been tentatively explained through recent experiments conducted essentially over noble metals in the presence and absence of oxygen. The strength of the metal–NO bond appears to be essential and may determine the nature of the elementary steps for formation of the reaction products. To illustrate, the involvement of dimeric NO intermediates from weakly adsorbed NO species has been suggested for N_2O formation [18], whereas different routes for N_2 formation may occur between physisorbed NO molecules and reduced N-containing species (NH_{ads}) stabilised on Pt or between two identical intermediates. Regarding this latter proposal, the associative desorption of two adjacent chemisorbed N atoms is usually suggested according to step (8) in Fig. 1 [14,18], but unusual mechanisms involving two adjacent nitrosyl and/or NH_{ads} species also have been proposed [18]. Mechanism 1 in Fig. 1 was proposed by our group for depicting the partial pressure dependencies of the rate of NO reduction by H_2 on supported Pd catalysts, which accounts for the dissociation of chemisorbed NO molecules assisted by hydrogen. But alternative routes can be envisaged taking into account various N-containing adsorbates, such as NH_{ads}. As a matter of fact, the introduction of the UBI-QEP method provides some guidelines for selecting the most relevant elementary steps for depicting the NO/H_2 reaction on $Pt/LaCoO_3$; however, the theoretical values calculated from this phenomenological model integrate the pressure gap that usually differentiates surface science studies under ultra-high vacuum on single crystals and kinetic investigations at atmospheric pressure on polycrystalline catalysts.

It seems obvious that the predominant reaction sequence will be governed by the nature of the dissociation step of NO assisted by hydrogen, taking into account the involvement of the dissociated or molecular state for hydrogen. Among the various proposals presented in Table 2, the lowest activation barrier for NO dissociation was obtained with the assistance of dissociated hydrogen species ($NO_{ads} + H_{ads} \rightarrow N_{ads} + OH_{ads}$). Determining the successive

surface reactions leading to the formation of NH_3, N_2 and N_2O remains an open problem. As shown in Table 2, different routes can be considered involving N_{ads}, NH_{ads}, and NO_{ads} as intermediates. The N_2O-selectivity will be governed by the relative rates of those elementary steps depending on the rate constant (i.e., on the activation barrier) and also on the relative surface concentration of intermediates. The involvement of NH_{ads} species in the formation of N_2 and N_2O leads to lower values for ΔE than those calculated with N_{ads} as an intermediate. In this sense, considering the corresponding elementary steps could be relevant. However, the predominant formation of N_2O fits more correctly with the high activation barrier for the recombination of two adjacent N atoms and the limiting step $N_{ads} + H_{ads} \rightarrow NH_{ads}$ involved in the formation of ammonia. As suggested previously, mechanism 1 in Fig. 1 seems to be appropriate for depicting the NO/H_2 reaction over noble metals.

4.1. Mechanisms and rate expressions according to surface modifications of $Pt/LaCoO_3$

As observed, a decrease in the apparent energy of activation from 52.8 to 46.0 kJ mol^{-1} occurred when the reductive pretreatment was performed at higher temperatures. A rate expression can be derived from mechanism 1 based on the following set of assumptions: (i) NO dissociation as rate-determining, (ii) fast adsorption of the reactants at equilibrium, and (iii) chemisorbed H atoms and NO molecules as the most abundant species. The following equation can be established:

$$r = r_1 = 2(r_{N_2O} + r_{N_2}) + r_{NH_3} \cong k_7 \theta^*_{NO} \theta^*_H = \frac{k_7 K_{NO} P_{NO} \sqrt{K_{H_2} P_{H_2}}}{(1 + K_{NO} P_{NO} + \sqrt{K_{H_2} P_{H_2}})^2} \quad (26)$$

with

$$\theta^*_{NO} = \frac{K_{NO} P_{NO}}{1 + K_{NO} P_{NO} + \sqrt{K_{H_2} P_{H_2}}} \quad (27)$$

and

$$\theta^*_H = \frac{\sqrt{K_{H_2} P_{H_2}}}{1 + K_{NO} P_{NO} + \sqrt{K_{H_2} P_{H_2}}}, \quad (28)$$

where k_n and K_i are respectively the kinetic constant associated with step (n) and the thermodynamic constant for the adsorption of the compound i (i = NO and H_2), and θ^*_i represents the adsorbate coverage on metallic Pt particles.

The lower apparent activation energy recorded on $Pt/LaCoO_3$-(450) [46.0 vs 52.8 kJ mol^{-1} on $Pt/LaCoO_3$(250)] may have a different significance. It likely reflects changes in the nature of interactions between metallic Pt particles and the support due to significant structural changes. According to the extent of such interactions, the adsorptive properties of Pt can be altered. Consequently, activity and N_2O selectivity changes can be explained based on mechanism 1, taking into account significant modifications in the relative rates of each elementary step. Alternately, the creation of different active sites localised at the metal–support interface could explain changes in the apparent activation energies and the observation of an additional low-temperature conversion range as observed from TPR experiments. Such a viewpoint has been extensively developed for reducible supports, particularly when noble metal interacts with ceria and/or ceria/zirconia materials [31–33]. As a matter of fact, previous investigations of CO + O_2 on Pt/CeO_2 revealed a beneficial effect of ceria on Pt, explained by a weakening of the Pt–CO bond when platinum interact with reduced ceria, and also a charge transfer from metal to ceria, accompanied by a slight increase in the oxidation state of the metal and a decrease in the Ce–O bond strength correlatively [33]. Accordingly, a cooperative effect between Pt and CoO_x segregated after extensive reduction of $LaCoO_3$ could explain our results. Previous studies proposed those beneficial effects for depicting $NO/H_2/O_2$ in the interaction of noble metals and reducible supports. It was proposed that ad-NO_x species stored on the support would react with chemisorbed H atoms at the metal–support interface [34,35]. Under our conditions, those ad-NO_x species were not observed by XPS, and no significant production of gaseous NO_2 was detected in the absence of O_2. Thus, the bifunctional mechanism shown in Fig. 1 seems more appropriate for the competitive adsorption of NO and H_2 on Pt and the involvement of the redox properties of CoO_x related to the formation of anionic vacancies (V), which can be further replenished via the dissociation of chemisorbed NO molecules on Pt according to steps (16)–(17) and (18), respectively. We note that the steps for the formation of N_2, N_2O, and NH_3 were similar on both mechanisms and involved Pt as active sites. Eqs. (29)–(31) can be easily derived based on previous assumptions. First,

$$r = r_2 = k_{18} \theta^*_{NO} \theta_V, \quad (29)$$

$\theta_V = 1 - \theta_O$ denotes the fraction of surface anionic vacancies, θ_O corresponds to the surface oxygen species from the support, and θ^*_{NO} represents the NO coverage on Pd particles. Steady-state approximation to anionic vacancies V from the support leads to

$$\theta_V = \frac{k_{16} \theta^*_H}{k_{18} \theta^*_{NO} + k_{16} \theta^*_H}. \quad (30)$$

Clearly, two different mechanisms may coexist that are difficult to differentiate unambiguously. Consequently, we considered both mechanisms 1 and 2, involving only noble metals and accounting for the existence of elementary steps on the reduced support. Consistently, the following can be derived:

$$r = r_1 + r_2 = k_7 \theta^*_{NO} \theta^*_H + k_{18} \theta^*_{NO} \theta_V = \frac{k_7 K_{NO} P_{NO} \sqrt{K_{H_2} P_{H_2}}}{(1 + K_{NO} P_{NO} + \sqrt{K_H P_{H_2}})^2} + \frac{k_{18} k_{16} K_{NO} P_{NO} \sqrt{K_{H_2} P_{H_2}}}{(k_{18} K_{NO} P_{NO} + k_{16} \sqrt{K_{H_2} P_{H_2}})(1 + K_{NO} P_{NO} + \sqrt{K_{H_2} P_{H_2}})}. \quad (31)$$

Numerical solutions for the kinetic k_n and thermodynamic K_i (i = NO and H_2) constants can be obtained through a statistical method described elsewhere [29] that involves minimising the sum of the square differences between calculated and experimental rates using the Solver setup on Microsoft Excel 5. As shown in Fig. 7, good correlation was observed between the experimental and predicted rates according to Eq. (31). The adjusted values for the parameters k_n and K_i are reported in Table 5. Different conclusions can be drawn from their examination and subsequent comparisons with those optimised earlier on $Pd/LaCoO_3$. As illustrated, $Pt/LaCoO_3$ behaved differently with significant changes in the rate constants involving steps on Pt and on the support. In addition, k_{18} was negligible on $Pt/LaCoO_3$(250), leading to the approximate rate expression $r \cong r_1$ and demonstrating that mechanism 1 likely occurred at 145 °C. According to previous XPS observations, this result seems to agree closely with a preferential segregation of Co^{3+} on $Pd/LaCoO_3$(250), exhibiting a lower intrinsic activity than Co^{2+} [23]. Consequently, Pt would catalyse the NO/H_2 reaction. In contrast, the corresponding values of k_{16} and k_{18} adjusted on $Pt/LaCoO_3$(450) were substantially higher than the value of k_7. Based on that comparison, we estimated the relative contributions of mechanisms 1 and 2 on the predicted rates. As shown in Fig. 8, the contribution of mechanism 1 did not exceed 15%; consequently, the approximation $r \cong r_2$ could be considered. Similar trends were previously found on $Pd/LaCoO_3$, with a more significant contribution of mechanism 2 at lower temperature (T = 110 °C).

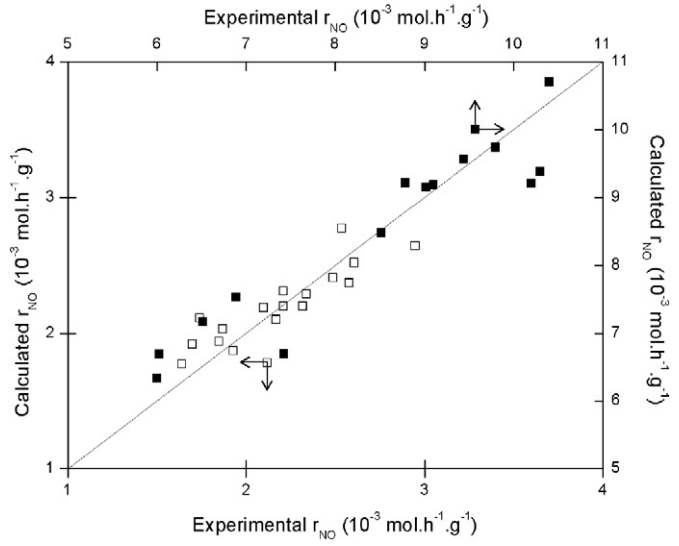

Fig. 7. Correlation between experimental and predicted rates on Pd/$LaCoO_3$(250) (■) and Pd/$LaCoO_3$(450) (□) according to Eq. and optimised parameters listed in Table 6.

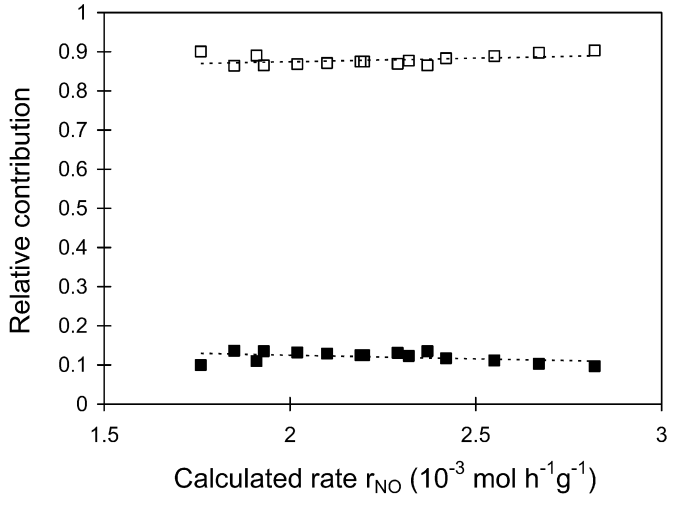

Fig. 8. Contribution of mechanism 1 (■) and 2 (□) for depicting the NO + H_2 reaction at 145 °C on Pd/$LaCoO_3$(450).

Returning to the temperature-programmed conversion profiles on Pt/$LaCoO_3$(450) and Pd/$LaCoO_3$(450), we note that they characterise different kinetic behaviours with the occurrence of two conversion regimes on Pt, in contrast to Pd. A tentative explanation for this may be based on comparing the relative rate constant k_{18}/k_{16} at 145 °C. The values of 12 and 59 on Pt/$LaCoO_3$(450) and Pd/$LaCoO_3$(450), respectively, indicate a substantially higher relative surface concentration of anionic vacancies on Pd/$LaCoO_3$(450) than on Pt/$LaCoO_3$(450). This comparison correctly explains the coexistence of mechanisms 1 and 2 on Pt/$LaCoO_3$(450), whereas only mechanism 2 would prevail on Pd/$LaCoO_3$(450) [13]. A borderline case where $\theta_V \ll \theta_O$ on Pt/$LaCoO_3$(450) at a sufficiently high temperature can be assumed. In such a situation, the contribution r_2 on the overall rate of NO conversion would become negligible with $r \cong r_1$. Such an assumption would satisfactorily explain the observation of two distinct conversion ranges on Pt/$LaCoO_3$(450), with the predominance of mechanism 1 at high temperature. Accordingly, a more extensive interaction would occur between Pd and the reduced support, which may explain changes in kinetic behaviour. Such an explanation seems to be in relative good agreement with the highest metal dispersion on Pd/$LaCoO_3$(450) [0.16 vs 0.06 on Pt/$LaCoO_3$(450)] corresponding to a larger interface.

We next consider changes in the adsorptive properties of noble metals. The comparison of the adsorption equilibrium constants in Table 5 shows that the competition for adsorption was usually in favour of NO, but the extent of such competition varied according to the nature of noble metals and the temperature of the prereductive thermal treatment. We note that those results corroborate previous theoretical calculations with higher values for the adsorption enthalpies of NO on Pt(111) and Pd(111) (see Table 2). More obvious is the comparison of K_{NO}/K_{H_2} equal to 32 and 7 on Pd/$LaCoO_3$(450) and Pt/$LaCoO_3$(450), respectively. Subsequently, the highest surface concentration of chemisorbed hydrogen atoms on Pt can be associated with a more extensive ammonia production, particularly as seen on Pt/$LaCoO_3$(450).

4.2. The nature on elementary steps for the production of nitrogen

As reported previously, S_{N_2O} depends on the relative rates r_{N_2}/r_{N_2O} and r_{NH_3}/r_{N_2O}. Consider the relative rates r_{N_2}/r_{N_2O} defined by Eq. (32),

$$\frac{r_{N_2}}{r_{N_2O}} = \frac{k_8}{k_{10}}\frac{\theta_N}{\theta_{NO}} + \frac{k_9}{k_{10}}. \tag{32}$$

θ_N/θ_{NO} can be obtained by applying the steady-state approximation to chemisorbed N atoms according to Eq. (33),

$$\frac{d\theta_N}{dt} = 0 = k_7\theta_{NO}\theta_H - 2k_8\theta_N^2 - (k_9 + k_{10})\theta_{NO}\theta_N - k_{11}\theta_N\theta_H. \tag{33}$$

Then Eq. (34) can be obtained after resolution and rearrangement,

$$\frac{\theta_N}{\theta_{NO}} = \frac{(k_9 + k_{10}) + k_{11}\theta_H/\theta_{NO}}{4k_8} \times \left(\sqrt{1 + \frac{8k_8k_7\theta_H/\theta_{NO}}{[(k_9 + k_{10}) + k_{11}\theta_H/\theta_{NO}]^2}} - 1\right). \tag{34}$$

Subsequent approximation can be achieved considering a surface covered predominately by chemisorbed NO molecules and considering previous assumptions. Equation (35) is thus obtained:

$$\frac{\theta_N}{\theta_{NO}} = \frac{(k_9 + k_{10})}{4k_8}\left(\sqrt{1 + \frac{8k_8k_7\sqrt{K_HP_{H_2}}}{(k_9 + k_{10})^2K_{NO}P_{NO}}} - 1\right). \tag{35}$$

The substitution of Eq. (35) in Eq. (32) leads to Eq. (36),

$$\frac{4r_{N_2}}{r_{N_2O}} + 1 = \frac{k_9 + k_{10}}{k_{10}}\sqrt{1 + \frac{8k_8k_7\sqrt{K_HP_{H_2}}}{(k_9 + k_{10})^2K_{NO}P_{NO}}} + \frac{3k_9}{k_{10}}. \tag{36}$$

The weak partial pressure dependency of the N_2O selectivity reported previously on Pd/$LaCoO_3$ [12] can be easily explained if the ratio $8k_8k_7\sqrt{K_HP_{H_2}}/(k_9 + k_{10})^2K_{NO}P_{NO}$ is small, which implies high numerical solutions for K_{NO}, k_9, and k_{10} compared with those obtained for K_H, k_8, and k_7. In such a case, Eq. (36) can be simplified, leading to Eq. (37):

$$\frac{r_{N_2}}{r_{N_2O}} \cong \frac{k_9}{k_{10}}, \tag{37}$$

with $k_9/k_{10} = 0.33$. This result is consistent with very low values for θ_N compared with θ_{NO} in all cases. Consequently, the rate of the recombination of two chemisorbed N atoms (step (8)) likely would be much slower than those of steps (9) and (10), and the production of N_2 would involve mainly step (9). Such a relative weak sensitivity to reaction conditions was not observed on Pt/$LaCoO_3$(450) and Pt/$LaCoO_3$(250) with a partial pressure dependency of N_2O selectivity (see Tables 5 and 6). Consequently, Eq. (37), previously established according to mechanism 1, could not be considered,

Table 5
Optimised kinetic and thermodynamic parameters calculated for the NO + H_2 reaction on Pt/$LaCoO_3$ at 145 °C

Catalyst	Temperature of reduction	k_7[a]	k_{16}[a]	k_{18}[a]	K_{NO} (atm^{-1})	K_H (atm^{-1})
Pt/$LaCoO_3$	250	$(3.1 \pm 0.5) \times 10^{-1}$	$(2.0 \pm 0.3) \times 10^{-2}$	≅0	85 ± 13	3 ± 0.5
	450	$(5.3 \pm 0.8) \times 10^{-3}$	$(1.2 \pm 0.2) \times 10^{-2}$	$(1.4 \pm 0.2) \times 10^{-1}$	200 ± 30	30 ± 5
Pd/$LaCoO_3$[b]	250	4.48			239	0.3
Pd/$LaCoO_3$[b]	450	≅ 0	2.1×10^{-2}	1.24	48	1.5

[a] $mol\,h^{-1}\,g^{-1}$.
[b] Calculated values from optimised kinetic and thermodynamic parameters in Refs. [12,13].

Table 6
Relative rate constant associated with the production of N_2 and N_2O during the NO + H_2 reaction on Pd/$LaCoO_3$(250) at 145 °C

Catalyst	Slope[a]	Intercept[a]	$k_8/(k_9+k_{10})^2$	k_9/k_{10}
Pt/$LaCoO_3$(250)	1.9×10^{-2}	0.24	0.15	0.24
Pd/$LaCoO_3$(250)[b]	≅0	0.33	≅0	0.33

[a] From the plot r_{N_2}/r_{N_2O} vs $\sqrt{p_{H_2}}/p_{NO}$.
[b] See Ref. [12].

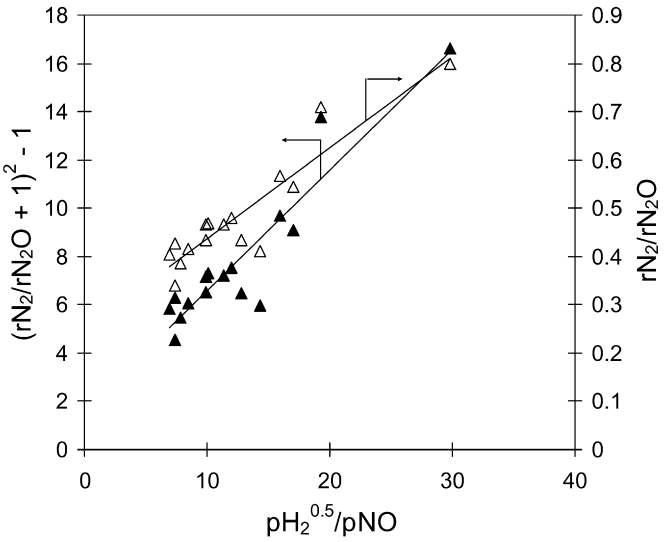

Fig. 9. Plot $(4r_{N_2}/r_{N_2O}+1)^2-1$ vs $\sqrt{P_{H_2}}/P_{NO}$ on Pt/$LaCoO_3$(250) from steady-state rate measurements at 145 °C.

particularly on Pt/$LaCoO_3$(250). In an initial approach, we considered the hypothesis that k_9 could be substantially lower than k_{10}, which agrees with the fact that the bimolecular reaction between N_{ads} and NO_{ads} usually gives N_2O, whereas the production of N_2 occurs via the associative desorption of two adjacent nitrogen N atoms. Accordingly, Eq. (38) must be considered:

$$\left[\frac{4r_{N_2}}{r_{N_2O}}+1\right]^2-1=\frac{8k_8k_7\sqrt{K_H P_{H_2}}}{(k_9+k_{10})^2 K_{NO}P_{NO}}. \quad (38)$$

Strictly speaking, the validation of these previous assumptions implies a straight line with a zero intercept for the plot $(4r_{N_2}/r_{N_2O}+1)^2-1$ versus $\sqrt{P_{H_2}}/P_{NO}$. As illustrated in Fig. 9, Eq. (38) is invalidated, suggesting that step (9) contributes to the formation of nitrogen. However, the straight line obtained also indicates that the value for the ratio $8k_8k_7\sqrt{K_H P_{H_2}}/(k_9+k_{10})^2 K_{NO}P_{NO}$ should be low compared with k_9/k_{10}, allowing the transformation of Eq. (36) to Eq. (39):

$$\frac{r_{N_2}}{r_{N_2O}}=\frac{k_9}{k_{10}}+2\left(1+\frac{k_9}{k_{10}}\right)\frac{8k_8k_7\sqrt{K_H P_{H_2}}}{(k_9+k_{10})^2 K_{NO}P_{NO}}. \quad (39)$$

Table 6 reports the slope and intercept of the straight line from the plot r_{N_2}/r_{N_2O} versus $\sqrt{P_{H_2}}/P_{NO}$ with the corresponding values of k_9/k_{10} and $k_8/(k_9+k_{10})^2$ and compares these values with those calculated previously on Pd/$LaCoO_3$(250). As observed, the main observation is associated with the recombination of adsorbed nitrogen atom for the production of nitrogen on Pt/$LaCoO_3$(250), in contrast to Pd/$LaCoO_3$(250).

5. Conclusion

The present study provided an extensive kinetic investigation of the reduction of NO by H_2 on supported Pt catalysts on $LaCoO_3$. Two complementary experimental and theoretical approaches were combined to obtaining a proposed mechanism and reliable kinetic and thermodynamic values that can characterise the effect of support materials on the adsorptive properties and reactivity of intermediates on Pt. Our main findings can be summarised as follows:

Kinetic features were strongly influenced by the prereduction temperature of $LaCoO_3$. Extensive reduction at 450 °C led to peculiar interactions between Pt and CoO_x. A bifunctional mechanism likely occurred in the NO/H_2 reaction.

Prereduction under mild conditions at 250 °C preserved the structural properties of $LaCoO_3$. No cooperative effect was seen between metallic Pt particles and the support, and the NO/H_2 obeyed a Langmuir–Hinshelwood mechanism.

The adsorptive properties of Pt also differed, with competitive adsorption more in favour of hydrogen on Pt/$LaCoO_3$(450), correlated with more extensive formation of ammonia than on Pt/$LaCoO_3$(250).

Subsequent comparisons with Pd/$LaCoO_3$ showed that NO adsorbed more strongly on Pd than on Pt, also correlated with lower formation of ammonia and changes in the nature of elementary steps for the formation of nitrogen.

The associative desorption of two chemisorbed nitrogen atoms occurred on Pt/$LaCoO_3$, in contrast to Pd/$LaCoO_3$, where the probability of finding two adjacent N atoms was very low.

Acknowledgments

Funding was provided by the Region Nord-Pas-de-Calais through the Institut de Recherche en Environnement Industriel. F. Dhainaut thanks the Centre National de la Recherche Scientifique for the award of a doctoral fellowship.

References

[1] C.N. Costa, P.G. Savva, C. Andronikou, P.S. Lambrou, K. Polychonopoulou, V.C. Belessi, V.N. Stathopoulos, P.J. Pomonis, A.M. Efstathiou, J. Catal. 209 (2002) 456.
[2] I. Nova, L. Lietti, L. Castoldi, E. Tronconi, J. Catal. 239 (2006) 244.
[3] A. Ueda, T. Nakato, M. Azuma, T. Kobayashi, Catal. Today 45 (1998) 135.

[4] M. Engelmann-Pirez, P. Granger, L. Leclercq, G. Leclercq, Catal. Today 107–108 (2005) 315.
[5] J. Xu, R. Clayton, V. Balakotaiah, M.P. Harold, Appl. Catal. B 77 (2007) 395.
[6] I. Twagirashema, S.M. Frere, L. Gengembre, C. Dujardin, P. Granger, Top. Catal. 42–43 (2007) 171.
[7] I. Twagisrashema, M. Engelmann-Pirez, M. Frère, L. Gengembre, L. Burylo, C. Dujardin, P. Granger, Catal. Today 119 (2007) 100.
[8] N. Takahashi, K. Yamazaki, H. Sobukawa, H. Shinjoh, Appl. Catal. B 70 (2006) 198.
[9] C.N. Costa, A.M. Efstathiou, J. Phys. Chem. B 108 (2004) 2620.
[10] C.N. Costa, V.N. Stathopoulos, V.C. Belessi, A.M. Efstathiou, J. Catal. 197 (2001) 350.
[11] M. Uenishi, M. Tanigushi, H. Tanak, Appl. Catal. B 57 (2007) 267.
[12] F. Dhainaut, S. Pietrzik, P. Granger, Appl. Catal. B 70 (2007) 100.
[13] F. Dhainaut, S. Pietrzik, P. Granger, Catal. Today 119 (2007) 94.
[14] W.C. Hecker, A.T. Bell, J. Catal. 92 (1985) 247.
[15] B. Frank, G. Emig, A. Renken, Appl. Catal. B 19 (1998) 45.
[16] R. Burch, M.D. Coleman, J. Catal. 208 (2002) 435.
[17] A.A. Shestov, R. Burch, J.A. Sullivan, J. Catal. 186 (1999) 362.
[18] R. Burch, A.A. Shestov, J.A. Sullivan, J. Catal. 186 (1999) 353.
[19] H. Taguchi, S.I. Matsu-ura, M. Nagao, T. Choso, K. Kabata, J. Solid State Chem. 129 (1997) 60.
[20] J.M. Gatica, R.T. Baker, P. Fornasiero, S. Bernal, J. Kaspar, J. Phys. Chem. B 105 (2001) 1191.
[21] P. Granger, C. Dathy, J.J. Lecomte, L. Leclercq, M. Prigent, G. Mabilon, G. Leclercq, J. Catal. 173 (1998) 304.
[22] P. Trambouze, H. van Landghem, J.-P. Wauquier, Les Réacteurs Chimiques, Conception, Calcul, Mise en Oeuvre, Technip, Paris, 1984.
[23] J.P. Dacquin, C. Dujardin, P. Granger, J. Catal. 253 (2008) 37.
[24] E. Shustorovich, H. Sellers, Surf. Sci. Rep. 31 (1998) 1.
[25] E. Shustorovich, A.T. Bell, Surf. Sci. 289 (1993) 127.
[26] E. Shustorovich, A.T. Bell, Surf. Sci. 253 (1991) 388.
[27] J.L. Gland, B.A. Sexton, Surf. Sci. 94 (1980) 355.
[28] A.V. Zeigarnik, Kinet. Catal. 45 (2004) 561.
[29] Y.J. Mergler, B.E. Nieuwenhuys, Appl. Catal. B 12 (1997) 95.
[30] G. Meunier, F. Garin, J. Schmitt, G. Maire, R. Roche, Stud. Surf. Sci. Catal. 30 (1987) 243.
[31] H.C. Yao, Appl. Surf. Sci. 19 (1984) 398.
[32] C. Serre, F. Garin, G. Belot, G. Maire, J. Catal. 141 (1993) 9.
[33] C. Serre, F. Garin, G. Belot, G. Maire, J. Catal. 141 (1993) 1.
[34] G.L. Chiarello, D. Ferri, J.D. Grundwald, L. Forni, A. Baiker, J. Catal. 252 (2007) 137.
[35] C.N. Costa, A.M. Efstathiou, J. Phys. Chem. C 111 (2007) 3010.